Study of Laser Interaction with Thin Targets

C. D. Boley, K. P. Cutter, S. N. Fochs, P. H. Pax, M. D. Rotter, A. M. Rubenchik, R. M. Yamamoto

March 11, 2009

Disclaimer

This document was prepared as an account of work sponsored by an agency of the United States government. Neither the United States government nor Lawrence Livermore National Security, LLC, nor any of their employees makes any warranty, expressed or implied, or assumes any legal liability or responsibility for the accuracy, completeness, or usefulness of any information, apparatus, product, or process disclosed, or represents that its use would not infringe privately owned rights. Reference herein to any specific commercial product, process, or service by trade name, trademark, manufacturer, or otherwise does not necessarily constitute or imply its endorsement, recommendation, or favoring by the United States government or Lawrence Livermore National Security, LLC. The views and opinions of authors expressed herein do not necessarily state or reflect those of the United States government or Lawrence Livermore National Security, LLC, and shall not be used for advertising or product endorsement purposes.

Study of Laser Interaction with Thin Targets[*]

C. D. Boley, K. P. Cutter, S. N. Fochs, P. H. Pax,
M. D. Rotter, A. M. Rubenchik, and R. M. Yamamoto

Lawrence Livermore National Laboratory
Livermore, CA 94551

For many targets of interest, the thickness is small compared to the conduction length during the engagement. In addition, the laser-material interaction region can be treated as flat. We have studied this regime with our 25 kW solid-state laser. We have demonstrated that airflow can reduce by approximately 40% the energy required to break through a thin target. This reduction is caused by the bulging of the softened material and the tearing and removal of the material by aerodynamic forces. We present elastic modeling which explains these results.

Keywords: Solid-state laser, high average power, airflow, elasticity, aerodynamic force

Nomenclature

a	laser spot size
D	thermal diffusivity
E	Young's modulus
h	target thickness
p	pressure
T	temperature
U	wind speed
w	elastic deflection
Y	yield strength
α	optical absorptivity
κ	thermal conductivity
ν	Poisson's ratio
ρ	mass density
σ	stress

1. Introduction

The role of airflow in enhancing laser interactions with metals has been studied for some time[4,9,10]. In most cases, the enhancement is due to two factors. First, airflow removes the melted material, thus increasing the ablation rate. Second, airflow removes the oxide layer and provides an oxygen supply, thereby aiding the combustion process[10]. This paper analyzes an experiment in which a third mechanism -- aerodynamic pressure decrease -- plays a dominant role[3,8].

The experiment involves the irradiation of thin sheets of aluminum by a 25-kW solid-state laser, with a large spot size, of order several cm. Airflow produces a pressure difference between the front and rear part of the sheet. While laser heating softens the material, the pressure difference causes the aluminum to bulge into the wind, and thus into the incoming beam. The resulting shear stresses rupture the material and lead to its removal by the airflow, at temperatures well below its melting point. Combustion plays an insignificant role because a strong, dense oxide layer builds up on the aluminum surface.

After reviewing the experiment, we discuss the overall behavior of target burn-through, on the basis of high-speed photography and thermocouple data. We then turn to an elastic analysis, modeling the target as a clamped plate subject to the pressure differential set up by airflow. Combining the model with burn-through information, we are able to make estimates for the elastic modulus and yield strength of the target at the burn-through temperature.

2. Experimental Review

The experimental setup, as described in[1], is illustrated in Fig. 1. Sheets of aluminum 6061 (thickness 0.18 cm) were irradiated by a solid-state heat-capacity laser operating at a time-averaged power of about 25 kW and a wavelength of 1.064 μm. The laser produced pulses of energy about 125 J, at a pulse repetition rate of 200 Hz (for a time-averaged power of 25 kW). The pulse length was about 0.5 ms. Since the pulse-to-pulse period was 5 ms, the duty factor was about 10%. The beam footprint was square, and the intensity was practically uniform over the spot. Examination of the laser imprint after several pulses showed no visible patterns. According to calorimetry, the pulse-to-pulse energy varied by less than 5%.

The temperature response was close to that of a CW laser with the same average power. The reason is that the characteristic diffusion distance between pulses was of order $(4D\tau)^{1/2} \sim 0.1$ cm, where the thermal diffusivity has been estimated as $D \sim 1$ cm^2/s. This distance is small compared to the spot size of several cm. On the other hand, it is of the same order as the thickness of the sheet. Thus temperature uniformity is established very rapidly through the target thickness, regardless of the pulse format.

The wind blower generated airflow with a speed of about 100 m/sec along the target surface. The targets were painted black or standard military green with high absorptivity. Some experiments were done with bare aluminum sheets. The diagnostics included thermocouples attached to the target rear side, infrared cameras, and high-speed cameras to observe the development of surface modifications.

3. Overall Behavior

First we consider an experiment without airflow. Figure 2 shows a target having a spot size of 12x12 cm^2 (irradiance ~ 0.17 kW/cm^2), irradiated for 4 s. The sample exhibits both cracking and melting, but there is no burn-through.

In contrast, airflow results in a dramatic burn-through during the same irradiation time, as shown in the right-hand part of Fig. 2. Here the spot size is 13x13 cm^2 – somewhat larger than that above. The mechanism of breakup is clarified by the sequence of frames shown in Fig. 3. During the first second or so (not shown), the material is softened by the laser heating. Airflow decreases the pressure on the side of the incident beam by $p = (1/2)\rho U^2$, or about 0.06 bars. This sets up an elastic bulging, which is proportional to the ratio of the pressure to Young's modulus, as we show in the next section. The pressure is relatively small, but Young's modulus decreases markedly with temperature. The bulging is apparent even before 2 s, as seen in frame 1 of Fig. 3. Note that a small hole has formed on the downwind side of the target. We believe that this is connected with the fact that the flow pattern over a bulge can lead to the formation of downwind vortices. These serve to increase the local pressure and to cause large shear stresses. For a smaller spot size, the bulging is less pronounced and the material breaks through in the center.

As the bulging increases, the stresses tear through the softened material, creating two holes (frames 2 and 3). These coalesce into a single large hole (frame 4) before the target is completely destroyed (frame 5). In the last three frames, one can discern the removal of macroscopic pieces of metal. Referring back to Fig. 1, we see that the screen

has debris collected after the shot. This verifies the presence of large unmelted pieces of metal, confirming that the burn-through occurs below the melting point.

Figure 4 shows the thermocouple trace in this case, along with two other cases having a larger spot size (16x16 cm^2) and a smaller spot size (9x9 cm^2). The thermocouple was placed at the center of the back side. In all cases, the traces reach a maximum (while the beam is still on) at temperatures well below the aluminum melting temperature ($T_m \sim 660$ C). Note, however, that the trace for the 13x13 cm^2 spot starts to decrease somewhat after 2 s. This cannot be a signal of burn-through, since we saw in the previous figure that a downwind hole had already formed somewhat earlier. We infer that the thermocouple remained attached to the coupon for a short time after the hole was formed. Thus the maxima of the thermocouple traces give an overestimation of the burn-through time.

Analytical estimates of the temperature development, ignoring burn-through phenomena, are also shown in Fig. 4. These are based on a simple model in which the temperature is assumed uniform through the slab, lateral heat transport is neglected (because the diffusion distance during a 4-s run is small compared to the spot size), and the beam is spatially flat. Radiative cooling is of the order of a few W/cm^2, which is negligible in comparison with the laser irradiance of more than 250 W/cm^2. From turbulent boundary layer theory[6], the cooling rate due to airflow is also of this order. In a reasonable approximation, then, the beam steadily heats the volume beneath the irradiated spot, producing an aluminum temperature given by[1]

$$T(t) = \alpha P t / A h \rho C, \tag{1}$$

where α is the optical absorptivity, P is the laser power, A is the spot area, and ρC is the heat capacity per volume. Here the material parameters are approximated by estimates halfway between room temperature and melting. As shown in Fig. 4, this elementary model compares well with experiment while the thermocouple is attached.

Because the sample is destroyed well below the melting temperature, airflow serves to reduce the amount of energy needed to burn through the material. We can estimate the fractional reduction in energy required for burn-through in comparison with the absence of airflow (when the sample must be melted) as

$$f = (T_m - T_b)/(T_m - T_0) ,$$ (2)

where T_b is the burn-through temperature and T_0 is room temperature. Using a burn-through temperature of 400 C, we see that airflow reduces the required energy by about 40%.

4. Elastic Analysis

We now turn to the elastic behavior of the heated material. Because the elastic modulus of aluminum decreases rapidly with temperature, even a small pressure difference will deform the material. Only the softened material is affected. Thus the situation is equivalent to the deformation of a thin, square membrane with clamped edges, subjected to uniform pressure, as illustrated in Fig. 5. The deflection satisfies the biharmonic equation with a driving term proportional to the pressure and inversely proportional to Young's modulus[7,12]:

$$\nabla^2 \nabla^2 w(x, y) = \frac{12 p (1 - \nu^2)}{E h^3} ,$$ (3)

where v is Poisson's ratio (approximately 0.3 in our case, independent of temperature), and h is the thickness of the metal. The clamped solution can be written in the form

$$w(x,y) = \frac{a^4 p (1-v^2)}{E h^3} \sum_m [f_m(\xi)g_m(\eta) + f_m(\eta)g_m(\xi)], \qquad (4)$$

where the dimensionless functions f_m and g_m are given in the Appendix. These depend on the dimensionless coordinates $\xi = x/a$ and $\eta = y/a$, which range between -1/2 and +1/2. The index m runs over odd integers 1, 3,…. The deflection is illustrated in Fig. 6. This figure also shows that if the edges were freely supported, then the bulging would increase by about a factor of three.

The deflection increases with time, since Young's modulus decreases with increasing temperature. Thus the time dependence is strictly parametric. Note that the deflection is extremely sensitive to the spot size, increasing as a^4. Another important fact is that it increases as the square of the wind speed.

At the center of the plate, the sum in the deflection formula of Eq. (4) is approximately 0.0152. From Fig. 3, we see that the maximum bulging before burn-through is $w_0 \sim 1$ cm. Using the aerodynamic pressure drop of 0.06 bars noted earlier, we infer that the value of Young's modulus at burn-through is about 4 kbar. This represents a dramatic decrease of more than two orders of magnitude from the room-temperature value of about 700 kbars.

The stresses are obtained from the deflection by evaluating the strains and using the stress-strain relations. The nonzero components are σ_{xx}, σ_{yy}, and σ_{xy}. The first two

components are of primary interest to us, since the shear stress vanishes at the center of the plate. The *xx* component, on the outward bulging face, is

$$\sigma_{xx}(x,y) = -\frac{a^2 p}{2h^2} \sum_m \left\{ f_m''(\xi)g_m(\eta) + f_m(\eta)g_m''(\xi) + \nu[f_m(\xi)g_m''(\eta) + f_m''(\eta)g_m(\xi)] \right\}, (5)$$

and   follows from symmetry. The outer stress is tensile at the center and compressive at the edge, as shown in Fig. 7. It passes through zero at a normalized distance between 0.33 and 0.37, depending on the direction of the lineout.

Note that the stresses are independent of Young's modulus, as is consistent with dimensional analysis (*E* and *p* have the same units, and the thin-plate approximation forces the stresses to increase linearly with the latter). They are also independent of time. We take the point of view that burn-through occurs when the temperature-softened yield strength decreases to the point at which it satisfies the von Mises yield criterion[5] at the center:

$$Y^2 = \sigma_{xx}^2(0,0) + \sigma_{yy}^2(0,0). \qquad (6)$$

Thus the yield strength at the elevated temperature is given by $Y(T_b) = \sqrt{2}\,\sigma_{xx}(0,0)$. Since the sum in Eq. (5) is about -0.280 at the origin, we find $Y(T_b) \sim$ 60 bars. This should correspond to the ultimate yield strength at the burn-through temperature of approximately 400 C. According to approximate data[2], the ultimate yield strength decreases from about 3 kbar to 0.2 kbar, as the temperature increases from ambient to the vicinity of 400 C (Fig. 8). Our estimated value is about 30% of the high-temperature value. The level of agreement seems reasonable, given the unknown accuracy of the data and uncertainties in detecting the time of burn-through (and hence the burn-through temperature).

According to our estimate, the ratio of the yield strength at burn-through to the room-temperature value is about 0.02. We saw earlier that the corresponding ratio for Young's modulus was about 0.006. In some models[11], the two quantities have similar temperature dependences. Because of the great uncertainties involved, however, the level of agreement estimated here is reasonable.

5. Conclusions

We have analyzed an experiment involving the large-spot irradiation of thin sheets of aluminum by a 25-kW solid-state laser, in the presence of airflow at Mach ~0.3. As the material is softened by beam heating, the small pressure difference due to airflow causes the target to bulge into the wind. As a result, shear stresses rupture the material and lead to its removal, at a temperature below its melting point. Our analysis is based on high-speed photography, thermocouple data, and a detailed elastic model in which the target is treated as a clamped plate deformed by pressure.

For a 13x13 cm^2 spot, photography indicates that the target is first penetrated somewhat downwind of the center. In our interpretation, this is caused by vortices associated with the bulging. According to our elastic analysis, the bulging is extremely sensitive to spot size (the deflection increases as a^4). Therefore one might expect a smaller target, exposed to the same irradiance, to rupture not through vortices but through material softening at the center. From thermocouple data, the burn-through temperature for the 13x13 cm^2 spot was estimated to be 400 C, although it could be smaller because of a delay in detection.

From the calculated plate deflection, we inferred an estimate of Young's modulus at the burn-through temperature. This was more than two orders of magnitude less than

9

its room-temperature value. Similarly, the calculated stress led to an estimate of the

material strength at burn-through, which was of the same order as approximate material

data.

In the future, we hope to study the scaling with respect to both spot size and wind

speed. As we noted, substantial sensitivity can be expected in each case.

Appendix

The functions occurring in Eq. (4) are

$$f_m(\xi) = \frac{24\,(-1)^{(m-1)/2}\cos(2\alpha_m\xi)}{\pi^5\,m^2\cosh\alpha_m},$$

$$g_m(\xi) = g_m^{(a)}(\xi) + g_m^{(b)}(\xi),$$

$$g_m^{(a)}(\xi) = [\cosh\alpha_m - (1 + (1/2)\alpha_m\tanh\alpha_m)\cosh(2\alpha_m\xi) + \alpha_m\xi\sinh(2\alpha_m\xi)]/m^3,$$

$$g_m^{(b)}(\xi) = E_m\alpha_m[2\xi\sinh(2\alpha_m\xi) - \tanh\alpha_m\cosh(2\alpha_m\xi)],$$

where $\alpha_m = m\pi/2$. The first four constants in the last function are $E_1 = 0.3722$, $E_3 = $ -

0.0380, $E_5 = -0.0178$, and $E_7 = -0.0085$. We truncate the sum at four terms. If the

contribution $g_m^{(b)}(\xi)$ is dropped, then the solution reduces to that of a simply supported

plate under uniform pressure.

References

[1]Abbott, R. P., C. D. Boley, S. N. Fochs, L. A. Nattrass, J. M. Parker, A. M. Rubenchik, J. A. Smith, and R. M. Yamamoto, "High-Power Solid-State Laser: Lethality Testing and Modeling," 25th Annual Army Science Conference, Orlando, FL, Nov. 27 – 30, 2006.

[2]Aluminum Association, Inc., "Aluminum Design Manual," 3rd Ed., Jan. 2005.

[3]Beraun, J. E., "Laser Materials Effects," Short Course, Fifth Annual Directed Energy Symposium, Monterey, CA, Nov. 12, 2002; Beraun, J. E., and J. Evanoff, "Laser Effects and Vulnerability Assessment Process," Short Course, Sixth Annual Directed Energy Symposium, Albuquerque, NM, October 20, 2003.

[4]Crane, K. C. A., R. K. Garnsworthy, and L. E. S. Mathias, "Ablation of Materials Subjected to Laser Radiation and High-Speed Gas Flows," J. Appl. Phys. **51**, 5954-5961 (1980).

[5]Ford, H., and J. M. Alexander, "Advanced Mechanics of Materials," Longmans, Green and Co., London, 1963.

[6]Landau, L. D., and E. M. Lifshitz, "Fluid Mechanics," Pergamon Press, 1978.

[7]Landau, L. D., and E. M. Lifshitz, "Theory of Elasticity," 3rd Edition, Pergamon Press, Oxford, 1986.

[8]Mirels, H., and K. L. Zondervan, "Pulsed-Laser-Induced Vibration of Pressurized Thin Walled Cylinder**,"** AIAA Journal **44**, 128-135 (2006).

[9]Physical Sciences, Inc. (W. T. Laughlin, H. H. Legner, M. G. Miller, E. R. Pugh, and G. A. Simons), "Laser Materials Effects and Lethality Handbook," PSI-1302/TR-1615 (1999).

[10]Prokhorov, A. M., V. I. Konov, I. Ursu, and I. N. Mihailescu, "Laser Heating of Metals," Adam Hilger, 1990.

[11]Steinberg, D. J., S. G. Cochran, and M. W. Guinan, "A Constitutive Model for Metals Applicable at High Strain Rate," J. Appl. Phys. **51**, 1498 (1980).

[12]Timoshenko, S., and S. Woinowsky-Krieger, "Theory of Plates and Shells," 2nd Edition, McGraw-Hill Book Company, Inc., New York, 1959. References to the original literature are given here.
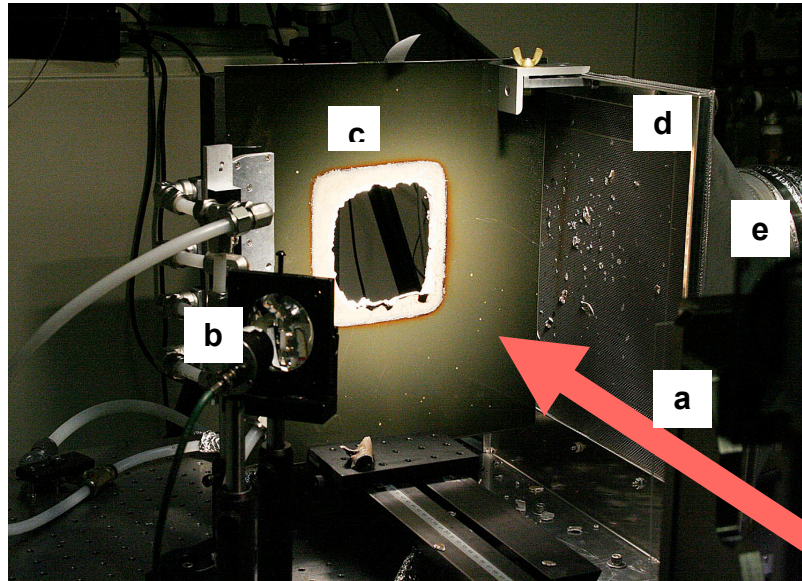
Figure 1. Experimental setup, immediately after irradiation of a target. The laser is out of view, to the lower right. The designated elements are: (a) beam path, (b) blower assembly, (c) target (in this case, a 13x13 cm^2 spot size), (d) coupon pieces on a screen, (e) suction assembly.
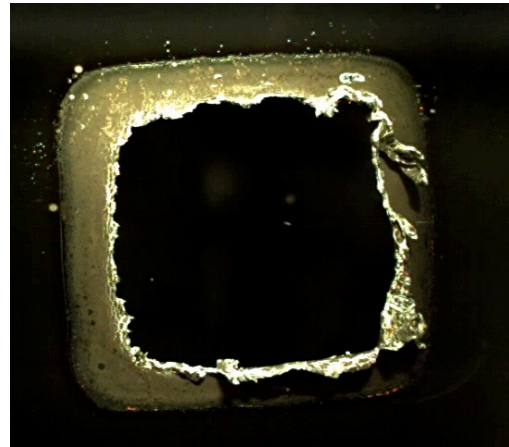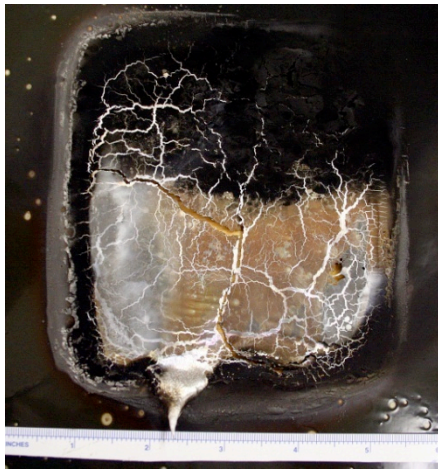
Figure 2. Two targets irradiated for 4 s. Left: 12x12 cm^2 spot, without airflow. Right: 13x13 cm^2 spot, with airflow.
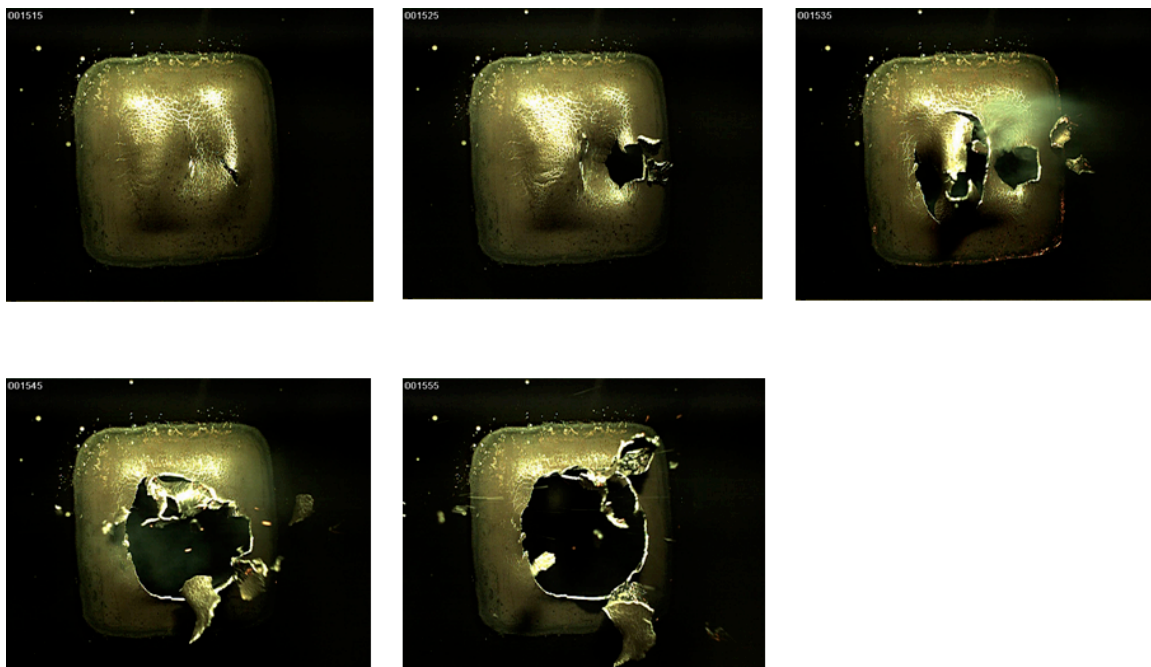
Figure 3. Successive stages in the burn-through of a 13x13 cm^2 aluminum target. The wind is from the left. The time of the first frame is 1.67 s after the beam was turned on. The time between frames is about 160 ms.
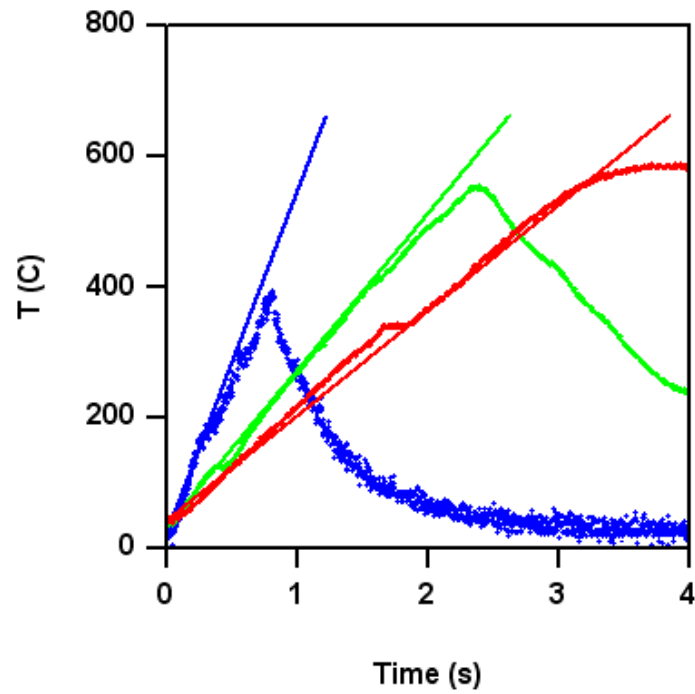
Figure 4. Thermocouple traces and thermal model results for three spot sizes: 16x16 cm^2 (red), 13x13 cm^2 (green), and 9x9 cm^2 (blue). The thermocouple traces are jagged, while the model results are straight lines.
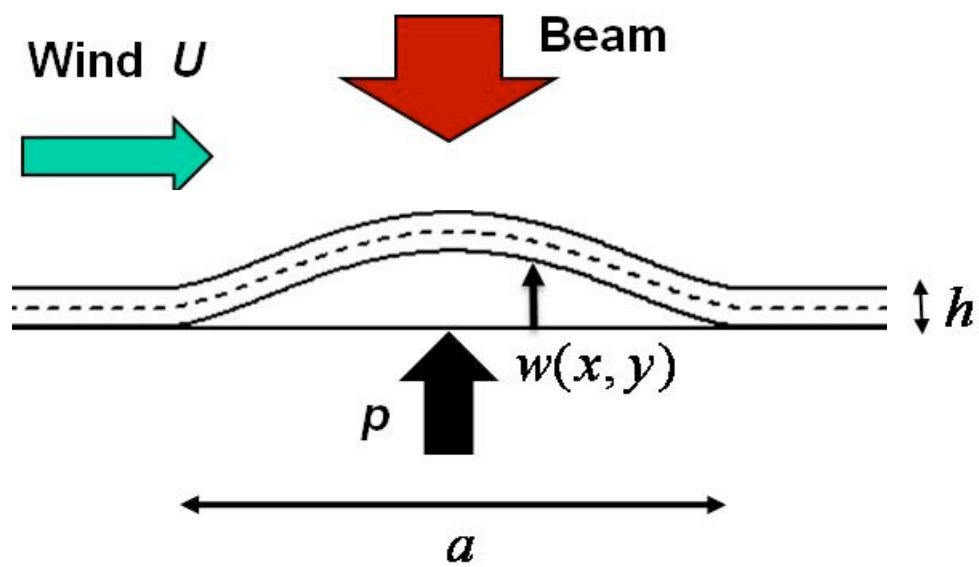
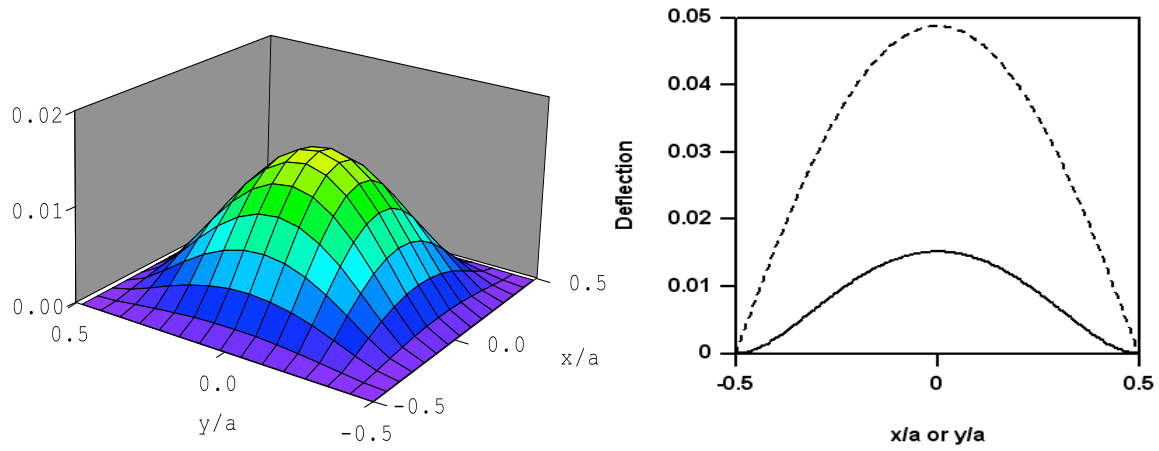**Figure 5.** Geometry of the elastic model (not to scale)

Figure 6. Calculated deflection of the target, versus normalized position The right-hand figure gives the horizontal (or vertical) lineout. The full line corresponds to a clamped plate, while the dashed line shows a freely supported plate. The deflection is normalized by $p\,a^4(1-v^2)/E h^3$.
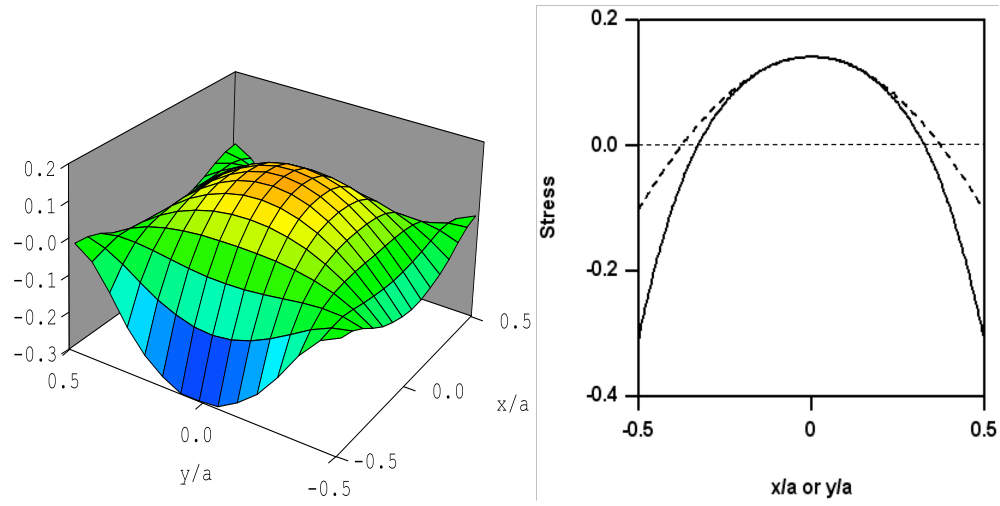
Figure 7. Calculated stress σ_{xx} on the outer face of the target, versus normalized position. Full line on the right: horizontal lineout; dashed line: vertical lineout. The stress is normalized by $p\,a^2\,/\,h^2$.
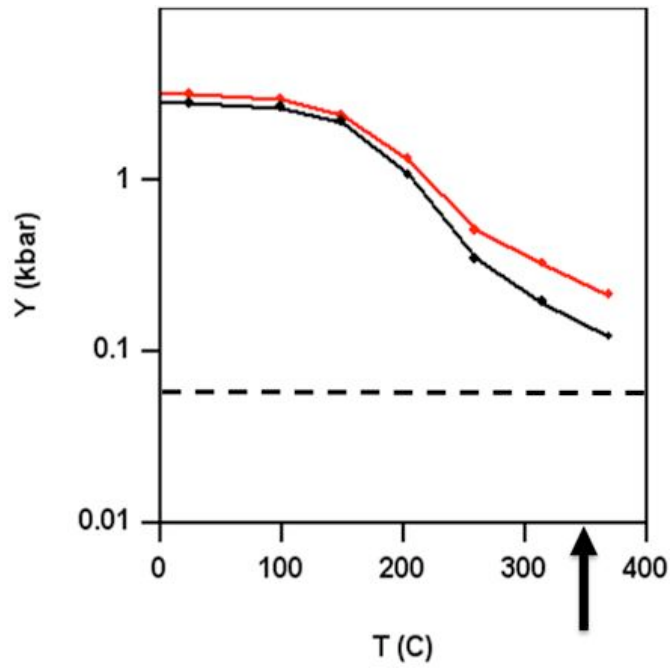
Figure 8. Ultimate tensile strength (red line) and yield tensile strength (full black line) of Al6061, as functions of temperature[2]. The data are subject to large uncertainties. The dashed line gives the yield stress (60 bars) estimated from target experiments. The arrow indicates the approximate burn-through regime.